2 Dimensional Electron Density Profiling of Plasma by Interferometry and Fringe Pattern Analysis

By Joseph A. OFOSU[1)], Kohei SHIMAMURA[1)], Kimiya KOMURASAKI[1)] and Hiroyuki KOIZUMI[2)]

[1)] *Department of Advanced Energy, Graduate School of Frontier Sciences, The University of Tokyo, Japan*
[2)]*Research Center of Advanced Science and Technology, The University of Tokyo, Japan*

Laser supported detonation (LSD) wave propagation properties have been studied extensively, among which is the profiling of the electron number density distribution. The analysis usually involves the attainment of a 1-D profile from a 2-D image pattern which could possible lead to the non-utilization of some information. In order to improve the accuracy of the analysis' results, the application of the Fourier Fringe Analysis has been proposed to be used for the attainment of a 2-D profile of the number density. This method also involves the use of the phase unwrapping algorithm which has also been extensively studied and utilized in other applications.

Key Words: Laser supported detonation (LSD), Fourier Fringe Analysis, 2D Phase Unwrapping, Electron number density distribution

Nomenclature

A	:	Area
c	:	speed of light in vacuum
e	:	electron charge magnitude
K_n	:	relative refractive index of neutral particle
m_e	:	electron mass
N	:	refractive index
n_e	:	electron number density
ε_o	:	permittivity of free space
λ	:	wavelength
φ	:	phase information
Ω	:	solid angle
Subscripts		
1	:	785 nm wavelength
2	:	470 nm wavelength

1. Introduction

A Laser propulsion system produces effective thrust during the laser supported detonation (LSD) regime at which energy conversion from optical to kinetic is efficient. Laser propulsion is an idea originally proposed by Kantrowitz[1)] and a typical application example is the Lightcraft by Myrabo[2)]. One of the significant motivations is cost reduction, as conventional chemical launch systems for space development projects are relatively expensive[3)].

LSD waves' propagation properties have been studied extensively[4)-7)], in order to understand its sustenance or termination conditions as well as its effect on thrust generation. One of the diagnostics approach used is the two wavelength Mach-Zehnder interferometry to profile electron number density distribution. These profiles are obtained most of the time for the 1-D case, although interferograms are obtained in 2-D. Thus it is possible that the result of this 1-D analysis of a 2-D image might not be a true representation of the density profile since some data are unutilized during the analysis process. A previous work of our laboratory, profiled the electron number density in 1-D[8)].

The aim of this study was to profile electron number density in 2-D using the Fourier fringe analysis technique. This study only applies the research results of this technique; the pioneers of whom are Takeda et. al[9)] and Bone et. al[10)].

2. Experimental Setup

A transversely excited atmospheric (TEA) CO_2 pulse laser with nominal energy of 10 J was used to produce plasma for the experiments. A joule meter was used to measure the pulse energy before and after the experiments. This was to ensure that the shot-to-shot pulse energy deviations were kept below ±5% throughout experimentation. The pulse shape of the laser was detected using a photon-drag detector (Hamamatsu photonics-B749) and is shown in Fig. 1. A diode pumped solid-state (DPSS) blue laser (continuous wave (CW), 470 nm, 20 mW) and an infra-red diode laser (CW, 785 nm, 100 mW) were the probe beams. A spatial filter was used to remove unnecessary multiple-order energy peaks and spatial noise before the beam traversed the interferometric arms of the experimental apparatus. Images of the laser induced plasma were taken using two (ICCD) cameras namely; iStar (Andor Tech. Inc., resolution 1,024×1,024 pixels, minimum exposure time of 2 ns) and Ultra 8 (DRS Tech., resolution 520×520 pixels, exposure time of 10 ns). A pulse delay generator (Stanford Research Systems, Inc., Model №: DG535, rise time: 2 ns) was used to synchronize the operations of both the CO_2 laser and the ICCD cameras.

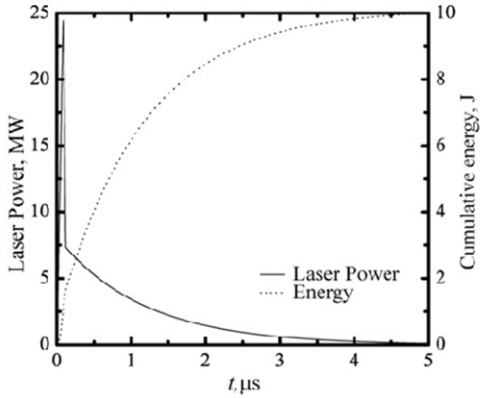

Fig. 1. Pulse shape of the CO_2 laser.

The schematic diagram for the two-wavelength Mach-Zehnder interferometer is as shown in Fig. 2. The near-infrared reflector was used to combine both beams into a single path before passing through the spatial filter. The two plano-convex lenses enabled the image of the propagating plasma to be projected visibly onto the ICCD devices. Both ICCD cameras were synchronized to capture the images at the same time using the pulse delay generator. This was verified using an oscilloscope to observe the trigger signals of both cameras. The temporal and spatial resolutions were 100 ns and 10 μm (for blue laser) and 12 μm (for infra-red laser) respectively. Two line filters with specifications: 470 nm ± 10 nm and 785 nm ± 2 nm were used to suppress the plasma emission. Figure 3 shows an example experimental image of the interferometer.

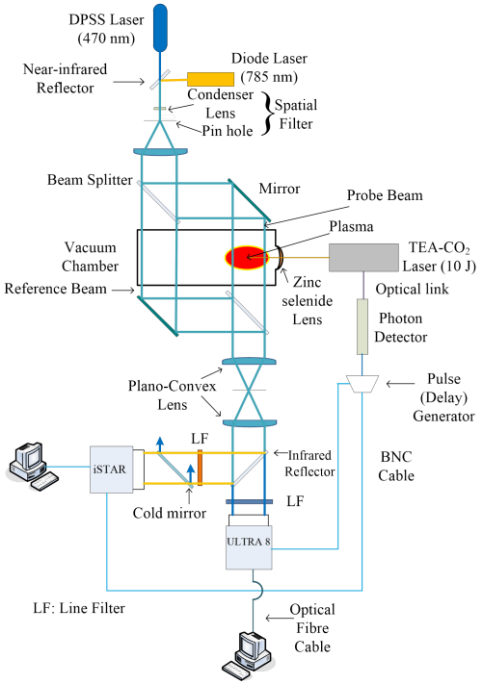

Fig. 2. Schematic of Mach-Zehnder interferometer.

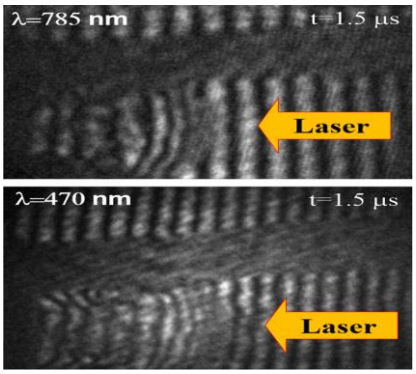

Fig. 3. Sample interferogram image taken at 1.5 μs.

3. Fourier Fringe Analysis

The Fourier fringe analysis technique has three different stages namely; the fringe pattern analysis (FPA), the phase unwrapping (PU) and the phase to refractive index stages. This is schematically shown in Fig. 4.

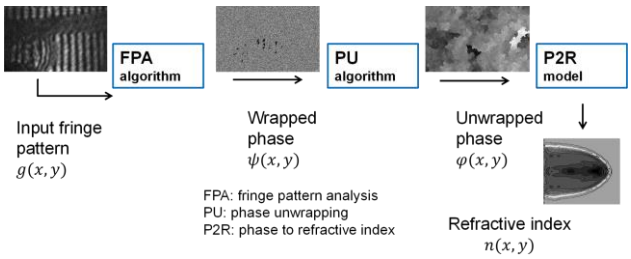

Fig. 4. Fourier Fringe Analysis Procedure

The interferogram obtained from the ICCD camera is the input for the FPA stage. The input can be defined as[9]:

$$g(x,y) = a(x,y) + b(x,y)\cos[2\pi(\alpha x + \beta y) + \varphi(x,y)] \quad (1.)$$

Where $a(x,y)$ is the background illumination, $b(x,y)$ is the amplitude modulation of the fringe visibility, $\varphi(x,y)$ is the phase information and α and β represent the spatial carrier frequency in the x and y directions respectively. Eq. (1) can be re-written as:

$$g(x,y) = a(x,y) + c(x,y)e^{i2\pi(\alpha x+\beta y)} + c^*(x,y)e^{-i2\pi(\alpha x+\beta y)}, \quad (2.)$$

where,

$$c(x,y) = 0.5b(x,y)e^{i\varphi(x,y)} \quad (3.)$$

Applying 2D fast Fourier transform (FFT) to eq. (2), we have:

$$G(f_x,f_y) = A(f_x,f_y) + C(f_x-\alpha, f_y-\beta) + C^*(f_x+\alpha, f_y+\beta) \quad (4.)$$

The FFT process is schematically shown in Fig. 5.

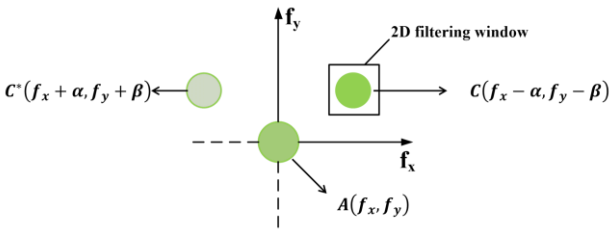

Fig. 5. The FFT process

The 2D window filter as seen in the above figure was achieved by a 2D Butterworth bandpass filter H_{BP} which is the convolution of a high and low pass filters. This is mathematically represented by the following equations:

$$H_{LP}\left(f_x, f_y\right) = \frac{1}{1+\left(D\left(f_x, f_y\right)/D_L\right)^{2n}} \quad (5a.)$$

$$H_{HP}\left(f_x, f_y\right) = 1 - \frac{1}{1+\left(D\left(f_x, f_y\right)/D_H\right)^{2n}} \quad (5b.)$$

$$H_{BP}(f_x, f_y) = H_{LP}(f_x, f_y) * H_{HP}(f_x, f_y) \quad (5c.)$$

After filtering and removal of the carrier frequencies, the signal is transformed back to the spatial domain using the inverse FFT to obtain $c(x,y)$. This is shown in Fig. 6.

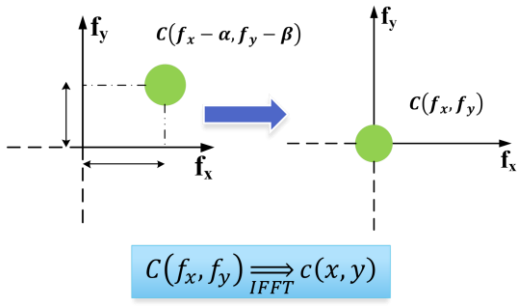

Fig. 6. Filtering and carrier frequency removal

The extraction of the phase $\varphi(x,y)$ requires the use of the four quadrant arctangent function which is designated as atan2. This function puts $\varphi(x,y)$ into a discontinuity of 2π phase jumps in the interval $(-\pi, \pi]$ and this is termed as phase wrapping. The wrapping function is defined as11):

$$\psi(x,y) = \text{atan2}\frac{Im\{c(x,y)\}}{Re\{c(x,y)\}} \quad (6.)$$

$$\psi(t) = \varphi(t) + 2\pi k(t) = \mathcal{W}(t) \quad (7.)$$

Where $k(t)$ is the integer function that wraps $\varphi(x,y)$. All the processes from the use of FFT, filtering, carrier frequency removal, IFFT and the application of atan2 to obtain $\psi(x,y)$ constitute the FPA stage. Figure 7 shows a sample of an input image and its wrapped phase output.

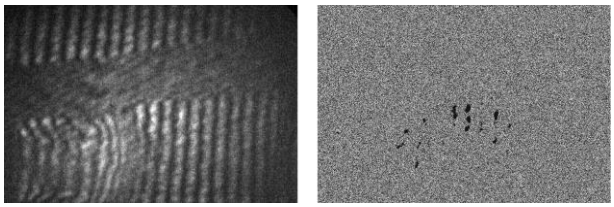

Fig. 7. Input image and wrapped phase output

Currently, 2 different algorithms are being considered in this study: Goldstein branch cut algorithm[11] and the 2D phase unwrapping algorithm based on sorting by reliability, following a non-continuous path (2D-SRNCP)[12]. Once the unwrapping is achieved, then the true phase $\varphi(x,y)$ would be related to the change in refractive index ΔN by the following equation:

$$\varphi(x,y) = \iint \Delta N \, \mathrm{dA} \quad (8.)$$

The electron number density n_e can be computed from estimated refractive index distributions at two separate wavelengths as shown in equation (9).

$$n_e = \left(\frac{8\pi^2 c^2 m_e \varepsilon_o}{e^2}\right)\left(\frac{\Delta N_1 - \Delta N_2}{\lambda_1^2 - \lambda_2^2}\right). \quad (9.)$$

4. Summary

We intend to profile n_e in 2-D using the Fourier fringe analysis technique. We are currently applying the Goldstein unwrapping algorithm[11] as well the 2D-SRNCP[12] algorithm to achieve the true phase $\varphi(x,y)$ from which the change in refractive index can be obtained for the determination of n_e.

References

1) Kantrowitz, A.: Propulsion to Orbit by Ground-Based Lasers, *Astronautics & Aeronautics*, **10** (1972), pp. 74-76.
2) Myrabo, L.N., Messitt, D.G. and Mead, F.B. Jr.: Ground and Flight Tests of a Laser Propelled Vehicle, AIAA Paper 98-1001, Reno (1998).
3) Collins, P.: The promise of electricity from space for world economic development, *Proceedings of 5th International Energy Conference*, **3** (1993), pp. 50–59.
4) Mori, K., Komurasaki, K. and Arakawa, Y.: Influence of the focusing f number on the heating regime transition in laser absorption waves, *Journal of Applied Physics*, **92**, 10 (2002), pp. 5663-5667.
5) Mori, K., Komurasaki, K. and Arakawa, Y.: Energy transfer from a laser pulse to a blast wave in reduced-pressure air atmospheres, *Journal of Applied Physics*, **95**, 11 (2004), pp. 5979-5983.
6) Mori, K., Komurasaki, K. and Arakawa, Y.: Threshold laser power density for regime transition of a laser absorption wave in a reduced-density air atmosphere, *Applied Physics Letters*, **88**, 121502 (2006).
7) Ushio, M., Komurasaki, K., Kawamura, K. and Arakawa, Y.: Effect of laser supported detonation wave confinement on termination conditions, *Shock Waves*, **18** (2008), pp. 35-39.

8) K. Shimamura, K., Hatai, K., Kawamura, K., Fukui, A., Fukuda, A., Wang, B., Yamaguchi, T., Komurasaki, K. and Arakawa, Y.: Internal structure of laser supported detonation waves by two-wavelength Mach-Zehnder interferometer, *Journal of Applied Physics*, **109**, 084910 (2011).
9) M. Takeda, H. Ina, and S. Kobayashi: Fourier-Transform Method of Fringe-Pattern Analysis for Computer-Based Topography and Interferometry, *J. Opt. Soc. Am.*, **72**, 156 (1981).
10) D. J. Bone, H. A. Bachor, and R. J. Sandeman: Fringe-pattern analysis using a 2-D Fourier transform, *Appl. Opt.*, **25**, 10, (1986), pp. 1653-1660.
11) D. C. Ghiglia, and M. D. Pritt: Two-Dimensional Phase Unwrapping: Theory, Algorithms and Software, *A Wiley Interscience Publication*.
12) M. A. Herraez, D. R. Burton, M. J. Lalor, and M. A. Gdeisat: A fast 2D phase unwrapping algorithm based on sorting by reliability, following a non-continuous path, *Applied Optics*, **41**, 35, (2002), pp. 7437-7444.